arXiv:2201.11025v3 [physics.acc-ph] 23 Feb 2022

Equilibrium parameters in coupled storage ring lattices and practical applications

V. Ziemann*

Department of Physics and Astronomy,

Uppsala University, Uppsala, Sweden†

A. Streun‡

Paul Scherrer Institut, CH-5232 Villigen, Switzerland§

(Dated: February 24, 2022)

Abstract

We calculate equilibrium emittances and damping times due to the emission of synchrotron radiation for coupled storage ring lattices by evaluating the projections of the commonly used synchrotron radiation integrals onto the normal modes of the coupled motion. Orbit distortion is included by calculating off-axis contributions to the radiation integrals. We provide explicit formulae for fast forward calculation, which have been implemented into the interactive lattice design code OPA.

PACS numbers: 29.20.Dh, 29.27.Bd, 41.60.Ap

* volker.ziemann@physics.uu.se

† Orcid ID https://orcid.org/0000-0002-6229-5620

‡ andreas.streun@psi.ch

§ Orcid ID https://orcid.org/0000-0002-0209-7358

I. INTRODUCTION

The emittance is one of the crucial quantities that determines the transverse beam dimensions and thus the performance of storage rings. In electron rings it is determined by the balance of damping and excitation due to the emission of synchrotron radiation [1]. For rings with negligible coupling between the transverse planes, the effect is quantified by the classical synchrotron radiation integrals [2, 3]. Coupling was initially described by a heuristic emittance coupling constant $\kappa = \varepsilon_y/\varepsilon_x$ where ε_x and ε_y are the horizontal and vertical emittance, respectively. With the increased performance of accelerators elaborate methods to calculate the emittance coupling were developed [4–6]. We complement these often elegant, but sometimes less intuitive methods, by a generalization of the radiation integrals to a coupled lattice.

The beam optics code OPA [7], written and maintained by one of the authors, is tailored to interactively design beam optical systems. Especially for the initial design phase, estimating the equilibrium beam properties from the optics of a non-periodic system, helps to guide the optimization; and this requires the evaluation of the radiation integrals, especially for intrinsically coupled lattices, such as Spiral-COSAMI [8].

We consider the normal mode parametrization of the coupled one-turn transfer matrix as introduced by Edward and Teng [9] and extended by Sagan and Rubin [10], and calculate the projection of the radiation integrals onto the corresponding normal modes. Note that we also implemented the algorithm in MATLAB using the software from [11] which is useful to validate and cross-check the software.

In the discussion and also with regard to practical implementation, we assume that all linear beam optical elements such as quadrupoles or dipoles are defined by their transfer matrices for the un-coupled elements and sandwiched between coordinate rotation matrices that describe their misalignment pertaining to coupling of the transverse planes (i.e. a skew quadrupole is represented by a quadrupole sandwiched between $\pm 45^\circ$ rotations).

We only consider transverse coupling and assume the longitudinal dynamics to be decoupled by adiabatic approximation, i.e. the synchrotron oscillation are considered slow compared to the betatron oscillations, and a particle's longitudinal momentum is assumed as a constant. Furthermore our analysis is based on highly relativistic, paraxial and large bending radius approximations as commonly used for high energy storage rings, where beam

properties are determined by synchrotron radiation effects.

We start with a brief reminder of the required beam dynamics formalism, then we calculate the radiation integral I_5 (in the notation of ref [2]) responsible for excitation of betatron oscillations followed by the evaluation of I_4 that describes damping. From these follow the equilibrium beam parameters of a coupled lattice. We proceed further including contributions from orbit excursions, which may be due to energy offsets or lattice imperfections. Finally we discuss implementation issues and present some applications.

II. NORMAL MODES AND DISPERSIONS

Transverse beam dynamics using coordinates $(x, x', y, y', \Delta E/E)$ is covered by 5×5 transfer matrices for elements and [circular] concatenations of elements:

$$\left(\begin{array}{c|c} R & \vec{V} \\ \hline 0 & 1 \end{array}\right) \tag{1}$$

with R the 4×4 transverse transfer matrix and $\vec{V}$ the 4-dimensional vector of dispersion production.

If R is the one-turn matrix of a storage ring, starting at an arbitrary longitudinal position, a normal mode decomposition may be found [9, 10]:

$$R = T^{-1}\mathcal{A}^{-1}\mathcal{O}\mathcal{A}T \tag{2}$$

where $\mathcal{O}$ is the matrix containing the eigen-tunes

$$\mathcal{O} = \begin{pmatrix} O_a & 0 \\ 0 & O_b \end{pmatrix} \quad \text{with} \quad O_{a,b} = \begin{pmatrix} \cos\mu_{a,b} & \sin\mu_{a,b} \\ -\sin\mu_{a,b} & \cos\mu_{a,b} \end{pmatrix} \tag{3}$$

and $\mathcal{A}$ is the matrix that contains the local normal-mode beta functions. It is given by

$$\mathcal{A} = \begin{pmatrix} \mathcal{A}_a & 0 \\ 0 & \mathcal{A}_b \end{pmatrix} \quad \text{with} \quad \mathcal{A}_{a,b} = \begin{pmatrix} \frac{1}{\sqrt{\beta_{a,b}}} & 0 \\ \frac{\alpha_{a,b}}{\sqrt{\beta_{a,b}}} & \sqrt{\beta_{a,b}} \end{pmatrix} \tag{4}$$

where the indices a and b label the two eigen modes. The coupling matrix T and its inverse T^{-1} are given by [10]

$$T = \begin{pmatrix} gI & -C \\ C^{+} & gI \end{pmatrix} \qquad \text{and} \qquad T^{-1} = \begin{pmatrix} gI & C \\ -C^{+} & gI \end{pmatrix}, \tag{5}$$

with the 2×2 identity matrix I and the 2×2 coupling matrix C. Its symplectic conjugate C^+ and the scalar g are given by

$$C^+ = C^{-1} \det C, \quad \text{and} \quad g^2 = 1 - \det C. \tag{6}$$

The periodic solution for the four-dimensional dispersion $\vec{D} = (\vec{D}_x, \vec{D}_y)^T = (D_x, D'_x, D_y, D'_y)^T$ is constrained by

$$\vec{D} = R\vec{D} + \vec{V} \tag{7}$$

which can be solved for $\vec{D}$ with the result

$$\vec{D} = (1 - R)^{-1}\vec{V} \ . \tag{8}$$

Thus $\vec{D}$ describes the periodic dispersion in physical space. The normal mode dispersion is given by

$$\vec{\mathcal{D}} = (\vec{\mathcal{D}}_a, \vec{\mathcal{D}}_b)^T = (\mathcal{D}_a, \mathcal{D}'_a, \mathcal{D}_b, \mathcal{D}'_b)^T = T\vec{D}. \tag{9}$$

Further application of matrix $\mathcal{A}$ gives the normal mode dispersion in normalized phase space:

$$\vec{\tilde{D}} = (\tilde{D}_1, \tilde{D}_2, \tilde{D}_3, \tilde{D}_4)^T = \mathcal{A}\vec{\mathcal{D}} = S^{-1}\vec{D} \tag{10}$$

$$\text{with} \quad S = (\mathcal{A}T)^{-1} = T^{-1}\mathcal{A}^{-1}. \tag{11}$$

We thus defined dispersion in three different coordinate systems, which we will use as it is convenient, and which are related as

$$\vec{\tilde{D}}\ \text{(normalized)} \quad \xleftarrow{\mathcal{A}} \quad \vec{\mathcal{D}}\ \text{(decoupled)} \quad \xleftarrow{T} \quad \vec{D}\ \text{(real space)}$$

Having laid out the theoretical framework and definition of notations we proceed to calculate the effect of quantum excitations on the normal modes.

III. QUANTUM EXCITATION

The stochastic nature of the emission of synchrotron radiation causes heating of the beam if the photons are emitted at locations with dispersion. In a planar un-coupled lattice the effect of the lattice parameters, such as beta function β and dispersion D is described by

$$\mathcal{H} = \beta_x D'^2_x + 2\alpha_x D_x D'_x + \gamma D^2_x \tag{12}$$

with $\gamma = (1+\alpha^2)/\beta$. The synchrotron radiation integral I_5 is closely related to $\mathcal{H}$ by

$$I_5 = \oint \mathcal{H}|h|^3 \, ds \ , \tag{13}$$

where $h = 1/\rho$ is the local curvature in the bending magnets, and the integral extends over one turn in the ring as discussed in chapter 7 of [3]. We follow the same logic to generalize the derivation to the coupled case and assume to know the dispersion in real space coordinates, $\vec{D}$ at every point in the ring and especially inside the dipoles, where we know that the emission of photons happens. This emission is characterized by an average loss, which causes damping and a fluctuating part u that has average energy value zero $\langle u \rangle = 0$ and squared expectation value u^2. Here $u = \Delta E/E$ is the relative energy deviation of a particle. We consider only one location and in a particular realization of the random process the energy loss at a given turn i will be denoted by u_i. We will use the statistical properties later on. In order to understand the excitation process we consider a single electron that travels on the closed orbit appropriate for its energy. After the emission process, the electron is still at the same place, but the orbit appropriate for its new energy is different, because of the finite dispersion at the location of emission. Consequently the electron will start oscillation around the new equilibrium orbit. The change of coordinates $\Delta\vec{x}$ at which it starts the oscillation are given by

$$\Delta\vec{x} = -u_i\vec{D} \tag{14}$$

and after traveling n turns with the chance of an emission process on each turn we expect the electron's position to be

$$\vec{x}_n = -\sum_{i=1}^{n} R^{n-i} u_i \vec{D} \ . \tag{15}$$

Using the parametrization from eq. 2 it is obvious that powers of the transfer matrix R^m can be evaluated by

$$R^m = T^{-1}\mathcal{A}^{-1}\mathcal{O}^m\mathcal{A}T \tag{16}$$

which can be interpreted in the following way. Reading from right to left: T removes the coupling, $\mathcal{A}$ turns the ellipses into circles, and then $\mathcal{O}$ takes care of the phase advance or tune for the specified number of turns m. Finally we move back from normalized phase space to real space by the inverses of $\mathcal{A}$ and T.

Returning to eq. 15 we simplify it by mapping the entire equation into normalized phase

space by left multiplying with $\mathcal{A}T$. We use the notation $\vec{\tilde{x}} = \mathcal{A}T\vec{x}$ and write

$$\vec{\tilde{x}}_n = -\mathcal{A}T\left(\sum_{i=1}^{n} R^{n-i}u_i\right)\vec{D} = -\left(\sum_{i=1}^{n}\mathcal{O}^{n-i}u_i\right)\mathcal{A}T\vec{D} = -\left(\sum_{i=1}^{n}\mathcal{O}^{n-i}u_i\right)\vec{\tilde{D}} \tag{17}$$

with $\vec{\tilde{D}}$ the dispersion vector mapped into normalized phase space from eq. 10. Equation 17 has a nice intuitive interpretation. Instead of every energy loss u_i producing a kick of magnitude $u_i\vec{D}$ in real space, it produces a kick of magnitude $u_i\vec{\tilde{D}}$ in normalized phase space that propagates by multiplying it with the rotation matrix $\mathcal{O}$ for a given number of turns and eventually all the kicks from the separate turns are summed up.

In order to calculate the emittance growth due to such a sequence of kicks we first need to specify which emittance we really mean. In the following we will use the emittances of the two normal modes. In the case of an uncoupled lattice this will revert to the common definition of emittances. Moreover, the emittances are the ensemble averages over the Courant-Snyder action variables J_a and J_b for the respective normal modes, labeled a and b. We start by writing the previous equation in 2×2 block matrix form

$$\begin{pmatrix}\vec{\tilde{x}}_{a,n}\\ \vec{\tilde{x}}_{b,n}\end{pmatrix} = -\sum_{i=1}^{n} u_i \begin{pmatrix} O_a^{n-i} & 0\\ 0 & O_b^{n-i}\end{pmatrix}\begin{pmatrix}\vec{\tilde{D}}_a\\ \vec{\tilde{D}}_b\end{pmatrix} = -\sum_{i=1}^{n} u_i \begin{pmatrix} O_a^{n-i}\vec{\tilde{D}}_a\\ O_b^{n-i}\vec{\tilde{D}}_b\end{pmatrix} \tag{18}$$

where $\vec{\tilde{x}} = (\vec{\tilde{x}}_a, \vec{\tilde{x}}_b)^T$. Here $\vec{\tilde{x}}_a$ are just the first two components of the vector $\vec{\tilde{x}}$ and $\vec{\tilde{x}}_b$ components three and four. The action variable for the first normal-mode after n turns is thus given by

$$J_{a,n} = \frac{1}{2}\vec{\tilde{x}}_{a,n}^T\vec{\tilde{x}}_{a,n}\ . \tag{19}$$

We now insert $\vec{\tilde{x}}_{a,n}$ from eq. 18 and arrive at

$$\begin{aligned} J_{a,n} &= \frac{1}{2}\sum_{i=1}^{n}\sum_{j=1}^{n} u_i u_j \vec{\tilde{D}}_a^T \left(O_a^{n-j}\right)^T O_a^{n-i}\vec{\tilde{D}}_a \\ &= \frac{1}{2}\sum_{i=1}^{n}\sum_{j=1}^{n} u_i u_j \vec{\tilde{D}}_a^T \left(O_a^{T}\right)^{n-j} O_a^{n-i}\vec{\tilde{D}}_a \\ &= \frac{1}{2}\vec{\tilde{D}}_a^T\sum_{i=1}^{n}\sum_{j=1}^{n} O_a^{j-i} u_i u_j \vec{\tilde{D}}_a \end{aligned} \tag{20}$$

where we use that the power of a transpose matrix equals the transpose of the matrix to the same power. Furthermore, the matrix O_a is a rotation matrix and therefore orthogonal. This implies that its transpose equals its inverse.

Now we consider the ensemble average over many particles. Since the emission of photons from turn to turn is uncorrelated and has rms magnitude u^2 as discussed before we have $\langle u_i u_j \rangle = u^2 \delta_{ij}$ which allows us to evaluate one sum and the other one sums over a constant u^2. We obtain

$$\langle J_{a,n} \rangle = \frac{1}{2} \vec{\tilde{D}}_a^T \sum_{i=1}^{n} \sum_{j=1}^{n} u^2 \delta_{ij} O_a^{j-i} \vec{\tilde{D}}_a = \frac{1}{2} \vec{\tilde{D}}_a^T \vec{\tilde{D}}_a n u^2 \tag{21}$$

and observe that the average action variable grows linearly with the number of turns n.

The magnitude of the term u^2 is the rms energy kick received by the beam. It is then given by the ratio of the rms spread of the emitted photons $\dot{N}\langle \varepsilon^2 \rangle$ and the beam energy E and is given by (Section 3.1.4 in [12])

$$u^2 = \dot{N}\langle \varepsilon^2 \rangle = \frac{55}{24\sqrt{3}} \frac{\varepsilon_c P_\gamma}{E^2} = \frac{4 c r_e}{3} C_q \frac{\gamma^5}{|\rho^3|} \tag{22}$$

with r_e being the classical electron radius, the constant C_q, and the critical photon energy ε_c given by

$$C_q = \frac{55\,\hbar c}{32\sqrt{3}\,mc^2} \qquad \text{and} \qquad \varepsilon_c = \frac{3\,\hbar c \gamma^3}{2\,|\rho|} \tag{23}$$

The radiated power is given by

$$P_\gamma = \frac{e^2 c^3}{2\pi} C_\gamma E^2 B^2 = \frac{c C_\gamma}{2\pi} \frac{E^4}{\rho^2} \qquad \text{with} \quad C_\gamma = \frac{4\pi r_e}{3(mc^2)^3}\ . \tag{24}$$

Integrating the action variable J_a over the circumference of the ring we collect the contributions of all the dipole magnets in the ring. This allows us to define a growth rate for the normal-mode action variable

$$\frac{d\langle J_a \rangle}{dt} = \frac{2}{3} C_q r_e \gamma^5 \oint \frac{\vec{\tilde{D}}_a^T \vec{\tilde{D}}_a}{|\rho^3|} ds = \frac{2}{3} C_q r_e \gamma^5 I_{5a} \tag{25}$$

and similarly for the other normal mode b. Here we implicitly define the radiation integral I_{5a} for the first normal mode. Comparing with the expressions in refs. [3, 12, 13] we observe that $\mathcal{H}_a = \vec{\tilde{D}}_a^T \vec{\tilde{D}}_a$ takes the place of the commonly used symbol $\mathcal{H}$ that occurs in the description of emittance growth in uncoupled rings. It is important to note, that only the absolute curvature of the bending field is used but not the direction of deflection, because it provides the energy fluctuations as the source of emittance, and the normal mode dispersions project this noise on to the transverse eigen-modes.

For an uncoupled lattice the coupling matrix T from eq. 5 is unity and the matrix $\mathcal{A}$ contains the conventional un-coupled beta functions. Using the first two components of

eq. 10 we can write

$$\begin{pmatrix} \tilde{D}_x \\ \tilde{D}'_x \end{pmatrix} = \mathcal{A}_x \begin{pmatrix} D_x \\ D'_x \end{pmatrix} = \begin{pmatrix} 1/\sqrt{\beta_x} & 0 \\ \alpha_x/\sqrt{\beta_x} & \sqrt{\beta_x} \end{pmatrix} \begin{pmatrix} D_x \\ D'_x \end{pmatrix}$$
$$= \begin{pmatrix} D_x/\sqrt{\beta_x} \\ \alpha_x D_x/\sqrt{\beta_x} + \sqrt{\beta_x} D'_x \end{pmatrix} \tag{26}$$

and multiplying with its transpose, $\mathcal{H}_x = \vec{\tilde{D}}_x^T \vec{\tilde{D}}_x$, yields eq. 12.

IV. DAMPING

The second consequence of the emission of synchrotron radiation is the damping of transverse oscillations. In dipole magnets synchrotron radiation is emitted and that emission is energy dependent with the recoil from the photons along the direction of motion of the electrons. Subsequently the energy is restored in a radio-frequency cavity, but only the longitudinal component of the momentum vector is increased. The joint effect of emitting and restoring the energy leads to overall damping. We thus proceed to determine the damping times of the two normal modes a and b and loosely follow the description from ref. [13].

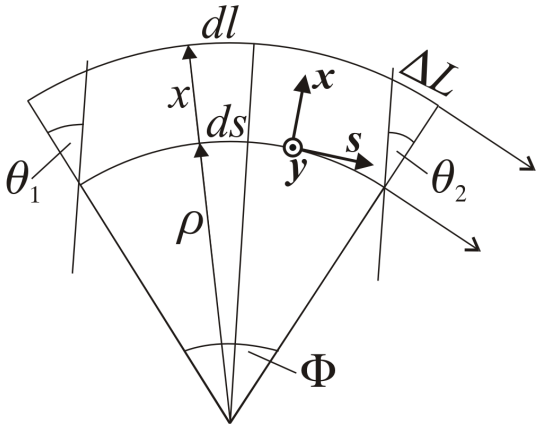


FIG. 1. Bending magnet geometry

In dipoles we denote the average emitted energy by $\Delta\bar{u}$ which is related to the power of the emitted synchrotron radiation P_γ by $\Delta\bar{u} = P_\gamma dl/cE$ where dl/c is a segment of the arc an electron travels in a magnet, see fig. 1, and P_γ is given in eq. 24.

If an electron suddenly changes its energy by an amount $\Delta\bar{u}$ due to photon emission, at a location with dispersion $\vec{D}$, its reference orbit will jump away from the electron and it will

perform betatron oscillations starting with $\Delta\vec{x} = -\vec{D}\Delta\bar{u}$ around the new reference orbit. Multiplying both $\Delta\vec{x}$ and the dispersion $\vec{D}$ by $\mathcal{A}T$ we obtain the effect on the normal modes

$$\Delta\vec{\tilde{x}} = -\vec{\tilde{D}}\Delta\bar{u} \tag{27}$$

and the action variables J_a and J_b will change by

$$\begin{aligned}\Delta J_a &= \tilde{x}_1\Delta\tilde{x}_1 + \tilde{x}_2\Delta\tilde{x}_2 = -\left(\tilde{x}_1\tilde{D}_1 + \tilde{x}_2\tilde{D}_2\right)\Delta\bar{u},\\ \Delta J_b &= \tilde{x}_3\Delta\tilde{x}_3 + \tilde{x}_4\Delta\tilde{x}_4 = -\left(\tilde{x}_3\tilde{D}_3 + \tilde{x}_4\tilde{D}_4\right)\Delta\bar{u}.\end{aligned} \tag{28}$$

We now need to determine the dependence of the energy loss $\Delta\bar{u}$ on the position in a combined function magnet with position-dependent magnetic field. We only consider an upright combined function magnet with only a horizontal dependence of the vertical field component. Other orientations or rotated magnets can easily be accommodated by coordinate rotations which enter the analysis by their influence on the coupling matrix T. Thus, without loss of generality, we describe the total average energy of the emitted photons by [13]

$$\Delta\bar{u} = -\frac{P_\gamma}{E}\frac{dl}{c} = -\frac{P_0}{cE}\left(1 + \frac{2}{B}\frac{\partial B}{\partial x}x\right)\left(1 + \frac{x}{\rho}\right)ds \tag{29}$$

$$\approx -\frac{P_0}{cE}\left(1 + \frac{2}{B}\frac{\partial B}{\partial x}x + \frac{x}{\rho}\right)ds \tag{30}$$

where x denotes the horizontal coordinate in the lab system, and P_0 is the power radiated on the design orbit. The term with the derivative of the magnetic field arises from the quadratic dependence of the emitted power on the magnetic field, see eq. 24, and the second term with x/ρ describes the longer path of the electron in the magnet if it is further out with larger x, see fig. 1. In dipoles containing also a skew gradient we would need to add $(dBy/dy)y$ to $(dBy/dx)x$ and consistently carry through all following steps.

Expressing the horizontal coordinate x through the normalized normal mode coordinates $\tilde{x}$ by using the matrix S from eq. 11,

$$x = \sum_{i=1}^{4} S_{1i}\tilde{x}_i \tag{31}$$

allows us to write the change in the action variables as

$$\Delta J_a = \frac{P_0}{cE}\left(1 + \sum_{i=1}^{4}\left(\tilde{x}_1\tilde{D}_1 + \tilde{x}_2\tilde{D}_2\right)S_{1i}\left(\frac{2}{B}\frac{\partial B}{\partial x}\tilde{x}_i + \frac{\tilde{x}_i}{\rho}\right)\right)ds. \tag{32}$$

Averaging over the normal-mode phases denoted by angle brackets, we find

$$\langle \Delta J_a \rangle = \frac{P_0 ds}{cE} \left(\frac{2}{B} \frac{\partial B}{\partial x} + \frac{1}{\rho} \right) \left(S_{11} \langle \tilde{x}_1^2 \rangle \tilde{D}_1 + S_{12} \langle \tilde{x}_2^2 \rangle \tilde{D}_2 \right) , \tag{33}$$

where we use the fact that $\langle \tilde{x}_i \rangle = 0$ and $\langle \tilde{x}_i \tilde{x}_j \rangle = 0$ with $i \neq j$, since the phases are evenly distributed for a large number of particles. Moreover, the expressions $\langle \tilde{x}_1^2 \rangle = \langle \tilde{x}_2^2 \rangle = \langle J_a \rangle$ are valid for normalized coordinates such that we finally obtain

$$\begin{aligned} \langle \Delta J_a \rangle &= \frac{P_0 ds}{cE} \left(\frac{2}{B} \frac{\partial B}{\partial x} + \frac{1}{\rho} \right) \left[S_{11} \tilde{D}_1 + S_{12} \tilde{D}_2 \right] \langle J_a \rangle \\ \langle \Delta J_b \rangle &= \frac{P_0 ds}{cE} \left(\frac{2}{B} \frac{\partial B}{\partial x} + \frac{1}{\rho} \right) \left[S_{13} \tilde{D}_3 + S_{14} \tilde{D}_4 \right] \langle J_b \rangle , \end{aligned} \tag{34}$$

where we recover the uncoupled case by setting $S_{11} = 1$ and all other S_{1i} to zero. The expressions with the square brackets and the dispersions $\tilde{D}$ are the projections of the coupled dispersions on the normal modes and thus intuitively generalize the uncoupled formalism to the transversely coupled case. The first two elements of the first row of the matrix S from eqs. 4–11 can be evaluated to be $S_{11} = g\sqrt{\beta_a}$ and $S_{12} = 0$ such that we have

$$S_{11} \tilde{D}_1 + S_{12} \tilde{D}_2 = g \mathcal{D}_a \ . \tag{35}$$

with $\mathcal{D}_a$ from eq. 9. Since S maps back from normalized phase space to real space eq. 31 applies to the physical dispersion as well, and we have

$$D_x = \sum_{i=1}^{4} S_{1i} \tilde{D}_i = g \mathcal{D}_a + S_{13} \tilde{D}_3 + S_{14} \tilde{D}_4. \tag{36}$$

$\mathcal{D}_a$ is the (non-normalized) a-mode dispersion, the b-mode dispersion is not needed. We use eq. 35 immediately to simplify the equation for $\langle \Delta J_a \rangle$: we insert P_γ from eq. 24 and the definitions of curvature and focusing strength, $h = 1/\rho = B/(B\rho)$ and $k = (\partial B/\partial x)/(B\rho)$, where $k > 0$ identifies a horizontally focusing magnet.

$$\frac{\langle \Delta J_a \rangle}{\langle J_a \rangle} = \frac{C_\gamma E^4}{2\pi} \frac{1}{E} g \mathcal{D}_a (2kh + h^3) \, ds \, . \tag{37}$$

We proceed to express the constant $C_\gamma E^4 / 2\pi$ by the total emitted power U_0 and the second radiation integral, defined as $I_2 = \int h^2 ds$

$$U_0 = \frac{C_\gamma E^4}{2\pi} \oint h^2 \, ds = \frac{C_\gamma E^4}{2\pi} I_2 \tag{38}$$

and arrive at

$$\frac{\langle \Delta J_a \rangle}{\langle J_a \rangle} = \frac{U_0}{E} \frac{1}{I_2} g \mathcal{D}_a (2kh + h^3) \, ds \tag{39}$$

for the first normal mode. Considering eq. 36, the relative damping of the second normal mode amplitude is conveniently expressed by the damping of the first mode amplitude and the damping in the uncoupled case.

$$\frac{\langle \Delta J_b \rangle}{\langle J_b \rangle} = \frac{\langle \Delta J_x \rangle}{\langle J_x \rangle} - \frac{\Delta J_a}{J_a} \quad \text{with} \quad \frac{\langle \Delta J_x \rangle}{\langle J_x \rangle} = \frac{U_0}{E}\frac{1}{I_2} D_x (2kh + h^3)\, ds \tag{40}$$

where D_x is the first component of the real-space dispersion from eq. 8.

So far we have considered sector dipoles such that damping of betatron amplitudes is given by integrating eqs. 39–40 over the length of the magnet. If, on the other hand, a magnet edge is rotated by an angle θ relative to the edge of a pure sector magnet, with $\theta > 0$ approaching a rectangular bend (i.e. a bend where both edge angles are half the bend angle: $\theta_1 = \theta_2 = \Phi/2$), the path of a particle at position x is shortened by $\Delta L = -x \tan\theta$, see fig. 1, thus its energy loss is reduced compared to the energy loss of a particle on the design orbit by

$$\Delta \bar{u} = -\frac{P_0}{cE}\,(1 + 2k\rho x)\,\Delta L \approx \frac{P_0}{cE} x \tan\theta \ . \tag{41}$$

The corresponding change in the action variable is (cf. eq. 32)

$$\Delta J_a = -\frac{P_\gamma}{cE}(\tilde{x}_1 \tilde{D}_1 + \tilde{x}_2 \tilde{D}_2) \sum_{i=1}^{4} S_{1i} \tilde{x}_i \tan\theta. \tag{42}$$

Repeating the manipulations from eq. 32 to 39 gives

$$\frac{\langle \Delta J_a \rangle}{\langle J_a \rangle} = -\frac{U_0}{E}\frac{1}{I_2} g \mathcal{D}_a h^2 \tan\theta \ . \tag{43}$$

The relative change of the action variable in a combined function magnet is obtained by integrating eq. 39 along the design orbit and adding the edge-effects from eq. 43. After summing over all bending magnets in the lattice we write

$$\frac{\langle \Delta J_{a,b} \rangle}{\langle J_{a,b} \rangle} = \frac{U_0}{E}\frac{I_{4a,b}}{I_2}\,, \tag{44}$$

where we have introduced two variants of the fourth radiation integral I_{4a} and I_{4b}, one for each normal mode, which are given by an integral over all bending sectors and a sum over all edges:

$$\begin{aligned} I_{4a} &= \oint g(s)\mathcal{D}_a(s)(2h(s)k(s) + h(s)^3)\, ds - \sum_{k}^{\text{edges}} g_k \mathcal{D}_{ak} h_k^2 \tan\theta_k \\ I_{4b} &= I_4 - I_{4a} \ . \end{aligned} \tag{45}$$

I_4 is the well-known integral without coupling, and given by I_{4a} for $g = 1$:

$$I_4 = \oint D_x(s)(2k(s)h(s) + h(s)^3)\, ds - \sum_k^{\text{edges}} D_{xk} h_k^2 \tan\theta_k$$

which reproduces the well-known case (Section 3.1.4 in [12]). For a small rectangular magnet ($\theta_1 = \theta_2 = hL/2$) with constant field and length L, where the optical functions do not change much over the magnet, eq. 45 simplifies to $\Delta I_{4a} \approx 2g\mathcal{D}_a hkL$.

The second, and dominant, contribution to transverse damping comes from the restoration of the longitudinal momentum in the radio-frequency cavities. There, on average, the momentum corresponding to the total energy lost in one turn $\Delta p = -U_0/c$ is added to the longitudinal momentum of the electron, whereas the transverse momenta remain unchanged. Since the transverse angles are the ratio of transverse to the much larger longitudinal momentum, we find [13] that both transverse angles are reduced by $-U_0/E$. This effect affects both transverse coordinates equally and therefore also the coordinates of normalized phase space $\tilde{x}$, and we have

$$\Delta\tilde{x}_2 = -\tilde{x}_2 \frac{U_0}{E} \qquad \text{and} \qquad \Delta\tilde{x}_4 = -\tilde{x}_4 \frac{U_0}{E}\,, \tag{46}$$

which causes a change in the action variables ΔJ_a and ΔJ_b that, upon averaging over betatron phases, leads to

$$\left.\frac{\langle \Delta J_a\rangle}{\langle J_a\rangle}\right|_{RF} = \left.\frac{\langle \Delta J_b\rangle}{\langle J_b\rangle}\right|_{RF} = -\frac{U_0}{E} \tag{47}$$

for the relative variation of the action variable due to the acceleration in the cavities.

Combining the effect of acceleration and emission of synchrotron radiation from eqs. 39, 40 leads to the following expressions

$$\begin{aligned}\left.\frac{\langle \Delta J_a\rangle}{\langle J_a\rangle}\right|_{tot} &= -\frac{U_0}{E}\left(1 - \frac{I_{4a}}{I_2}\right)\\ \left.\frac{\langle \Delta J_b\rangle}{\langle J_b\rangle}\right|_{tot} &= -\frac{U_0}{E}\left(1 - \frac{I_{4b}}{I_2}\right)\,,\end{aligned} \tag{48}$$

where we have to keep in mind that this is the variation of the action during one turn in the storage ring which has the duration T_0. Thus we find for the damping times τ_a and τ_b for the two normal modes

$$\begin{aligned}\frac{d\langle J_a\rangle}{dt} \approx \frac{\langle \Delta J_a\rangle}{T_0} &= -\frac{U_0}{T_0 E}\left(1 - \frac{I_{4a}}{I_2}\right)\langle J_a\rangle = -\frac{2}{\tau_a}\langle J_a\rangle\\ \frac{d\langle J_b\rangle}{dt} \approx \frac{\langle \Delta J_b\rangle}{T_0} &= -\frac{U_0}{T_0 E}\left(1 - \frac{I_{4b}}{I_2}\right)\langle J_b\rangle = -\frac{2}{\tau_b}\langle J_b\rangle\end{aligned} \tag{49}$$

and we recover the well-known expression [1] for the damping time, but generalized to describe the damping of the normal modes. Note that the conventional damping time refers to the damping of the amplitude of betatron oscillations, whereas in eq. 49 we calculate the reduction of the action variable, which accounts for the factor two in the definition of the damping time. The terms in brackets are commonly called the damping partition numbers $\mathcal{J}$, which tell how the total damping is distributed among the two transverse and the longitudinal mode.

$$\mathcal{J}_{a,b} = 1 - \frac{I_{4a,b}}{I_2}. \tag{50}$$

As proven under very general conditions, which include coupling [14], the total damping is constant, and as a consequence the damping partition numbers always sum up to 4. For the longitudinal damping partition and the three damping times we thus get:

$$\mathcal{J}_e = 4 - \mathcal{J}_a - \mathcal{J}_b \qquad \text{and} \qquad \tau_{a,b,e} = \frac{2ET_0}{U_0 \mathcal{J}_{a,b,e}} \tag{51}$$

Moreover our finding $I_{4a} + I_{4b} = I_4$ implies that $\mathcal{J}_e$ does not change with transverse coupling.

V. EMITTANCE

In sections III and IV we derived the generalized quantum excitation and damping integrals I_5 and I_4 including coupling. The other three integrals I_1, I_2, I_3 do not depend on coupling. The integral $I_1 = \oint h(s) D_x(s)\, ds$ determines the energy dependent path length (momentum compaction). Here only the dispersion in the plane of deflection is required; the dispersion in the orthogonal plane does not affect the path length in first order. A coordinate rotation may perform the transformation to entry or exit of a bend oriented differently. The integrals $I_2 = \oint h(s)^2\, ds$ and $I_3 = \oint |h(s)|^3\, ds$ do not depend on any optical functions and are therefore not affected by coupling.

The equilibrium normal-mode emittances, which we identify as the ensemble average of the action variables $\varepsilon_{a,b} = \langle J_{a,b} \rangle$, are given by the balance of heating, as described by eq. 25 and damping in eq. 49 with the result

$$\varepsilon_a = C_q \gamma^2 \frac{I_{5a}}{I_2 - I_{4a}} \quad \text{and} \quad \varepsilon_b = C_q \gamma^2 \frac{I_{5b}}{I_2 - I_{4b}}\ . \tag{52}$$

These are the same expressions found for uncoupled rings with the exception that here we use the generalized radiation integrals that describe the projections of excitation and damping on to the normal modes.

Turning back to the general coupled case and given the normal-mode emittances and the decomposition of the transfer matrix it is straightforward to determine the beam matrix in real space from that in normalized phase space. With the normal-mode emittances ε_a and ε_b the beam sigma matrix in normalized phase space $\tilde{\sigma}$ is given by

$$\tilde{\sigma} = \begin{pmatrix} \varepsilon_a & 0 & 0 & 0 \\ 0 & \varepsilon_a & 0 & 0 \\ 0 & 0 & \varepsilon_b & 0 \\ 0 & 0 & 0 & \varepsilon_b \end{pmatrix} \tag{53}$$

and the transfer matrix $S = T^{-1}\mathcal{A}^{-1}$ transports the particles from normalized phase space back to real space such that the sigma matrix σ becomes

$$\sigma = S\tilde{\sigma}S^T \tag{54}$$

and the projected emittances can be extracted from σ by taking the determinant of the 2×2 blocks on the diagonal which are the square of the projected emittances $\hat{\varepsilon}_{x/y}$.

A parameter quantifying the coupling between the planes can be introduced either by taking the ratio of the the normal-mode emittances $\tilde{\kappa} = \varepsilon_b/\varepsilon_a$ or the projected emittances $\kappa = \hat{\varepsilon}_y/\hat{\varepsilon}_x$. Which to take in a particular case is a matter of taste or convenience.

Since I_3 is not affected by coupling, the common formula for the energy spread is reproduced using the longitudinal damping partition from eq. 51:

$$\sigma_e^2 = C_q\gamma^2\frac{I_3}{I_2\mathcal{J}_e} = C_q\gamma^2\frac{I_3}{2I_2 + I_{4a} + I_{4b}} = C_q\gamma^2\frac{I_3}{2I_2 + I_4} \tag{55}$$

Finally the r.m.s. bunch length follows with I_1 from the energy spread and the synchrotron tune Q_s (for $Q_s << 1$):

$$\sigma_s = \frac{I_1}{2\pi Q_s}\sigma_e. \tag{56}$$

Eqs. 54–56 give the 6-dimensional equilibrium beam parameters at any location in a coupled lattice. They are determined by the generalized radiation integrals together with transverse (magnet gradients) and longitudinal (RF voltage) focusing.

VI. ORBIT DISTORTION

Magnet misalignments, active steerers or a beam energy offset cause a deviation of the beam centroid (orbit) from the reference path, which is defined by the multipole centers. As a consequence the beam experiences transverse fields and gradients in all multipoles, i.e. all magnets act as small bending magnets and thus contribute to the radiation integrals via feed-down of fields and gradients at the orbit position. We do not explicitely consider skew multipoles instead they are realized by rotations of regular multipoles.

Defining $X(s)$, $Y(s)$ as the local orbit relative to the reference trajectory, the coordinates of a particle oscillating around the orbit are $(X+x)$ and $(Y+y)$. Keeping only linear, regular multipoles and using again curvatures (inverse bending radii) we define local curvatures

$$h_X = \left.\frac{B_y}{(B\rho)}\right|_{x,y=0} = h_0 + kX \qquad h_Y = -\left.\frac{B_x}{(B\rho)}\right|_{x,y=0} = -kY, \tag{57}$$

with h_0 the curvature of the reference trajectory and k the gradient.

Generalizing the preceding treatments to an arbitrary orbit, we first realize that the radiation integrals I_2, I_3, I_5 contain only the quantum emission term which is given by the absolute curvature. At the orbit it is given by

$$|h| = \sqrt{h_X^2 + h_Y^2} = \sqrt{h_0^2 + 2h_0kX + k^2(X^2+Y^2)}. \tag{58}$$

For the damping integral I_4 the variation of path length with offsets x, y to the displaced orbit at X, Y has to be considered. Using local orbit curvatures h_X, h_Y the path length is approximated by

$$dl \approx ds(1 + h_X x + h_Y y), \tag{59}$$

if we keep only linear terms in coordinates. We use dl as a generic symbol for a path length element and not as global variable.

As derived in sec. IV, I_4 depends on the radiated power as a function of transverse position, which is proportional to the local field squared, see eq. 24: the radiation on the orbit depends on the field at the orbit and the energy of the orbit. So the average relative energy of the emitted photons from eq. 29 is given by

$$\Delta\bar{u} = \frac{P_\gamma}{E}\frac{dl}{c} = \hat{C}\left[(h_X + kx)^2 + (h_Y - ky)^2\right] \cdot (1 + h_X x + h_Y y)\, ds \tag{60}$$

with $\hat{C} = C_\gamma E^3/(2\pi)$ and the path length element from eq. 59, now also including the relative offset to the orbit. The first bracket corresponds to the squared magnetic field at the location of the particle. Keeping only linear terms in the coordinates x, y we get

$$\Delta\bar{u} = \hat{C}\,(C_0 + C_x x + C_y y)\;ds, \quad \text{with} \tag{61}$$

$$C_0 = |h|^2 \tag{62}$$

$$C_x = h_X\,(|h|^2 + 2k)$$

$$C_y = h_Y\,(|h|^2 - 2k)$$

where we used eq. 57 and eq. 58. We insert 61 into eq. 28 describing the change of betatron amplitudes due to radiation emission. Further we insert eq. 31 expressing x in normalized coordinates $\tilde{x}_i$, and the corresponding expression for y:

$$\Delta J_a = \left(\tilde{x}_1\tilde{D}_1 + \tilde{x}_2\tilde{D}_2\right)\hat{C}\left[C_0 + C_x\sum_{i=1}^{4} S_{1i}\tilde{x}_i + C_y\sum_{i=1}^{4} S_{3i}\tilde{x}_i\right]ds\,. \tag{63}$$

Averaging over betatron phases (cf. treatments following eq. 32) and performing the corresponding procedure for J_b results in

$$\begin{aligned}\langle\Delta J_a\rangle &= \hat{C}\left[C_x\left(S_{11}\tilde{D}_1 + S_{12}\tilde{D}_2\right) + C_y\left(S_{31}\tilde{D}_1 + S_{32}\tilde{D}_2\right)\right]ds\,\langle J_a\rangle\\ \langle\Delta J_b\rangle &= \hat{C}\left[C_x\left(S_{13}\tilde{D}_3 + S_{14}\tilde{D}_4\right) + C_y\left(S_{33}\tilde{D}_3 + S_{34}\tilde{D}_4\right)\right]ds\,\langle J_b\rangle\end{aligned} \tag{64}$$

With the relations between normalized, decoupled and real space dispersions (see eqs. 35, 36 and the corresponding ones for D_y, $\mathcal{D}_b$) we get

$$\begin{aligned}\frac{\langle\Delta J_a\rangle}{\langle J_a\rangle} &= \hat{C}\left[C_x g\mathcal{D}_a + C_y\left(D_y - g\mathcal{D}_b\right)\right]ds\\ \frac{\langle\Delta J_b\rangle}{\langle J_b\rangle} &= \hat{C}\left[C_y g\mathcal{D}_b + C_x\left(D_x - g\mathcal{D}_a\right)\right]ds\end{aligned} \tag{65}$$

On the reference orbit ($X = Y = 0$) we get $C_x = h_0(2k + h_0^2)$, $C_y = 0$ and recover eq. 37. For a pure quadrupole we simply set $h_0 = 0$.

If the magnet has a rotated edge of angle θ, then the path is shortened by $\Delta L = -x\tan\theta$, see Fig. 1 – now the orbit at X is the reference. Using ΔL instead of $dl = ds(1 + h_X x + h_Y y)$ we repeat the calculations and arrive at an expressions that corresponds to eq. 62 for the edge angles:

$$\bar{C}_0 = 0 \qquad \bar{C}_x = -\tan\theta\,|h|^2 \qquad \bar{C}_y = 0 \tag{66}$$

TABLE I. Radiation integrals for a general bending magnet with curvature h_0 and focusing strength k including coupling and orbit distortions.

$$I_1 = \int (h_X D_x + h_Y D_y)\, ds \qquad I_2 = \int |h(s)|^2\, ds \qquad I_3 = \int |h(s)|^3\, ds$$

$$I_{4a} = \int \left[C_x(s) g\mathcal{D}_a(s) + C_y(s)\left(D_y(s) - g\mathcal{D}_b(s)\right)\right] ds - \sum_{i=1,2} \tan\theta_i \bar{C}_{xi} g\mathcal{D}_{ai}$$

$$I_{4b} = \int \left[C_y(s) g\mathcal{D}_b(s) + C_x(s)\left(D_x(s) - g\mathcal{D}_a(s)\right)\right] ds - \sum_{i=1,2} \tan\theta_i \bar{C}_{xi}\left(D_{xi} - g\mathcal{D}_{ai}\right)$$

$$I_{5a} = \int \vec{\tilde{D}}_a^T(s) \cdot \vec{\tilde{D}}_a(s)\, |h(s)|^3\, ds \qquad I_{5b} = \int \vec{\tilde{D}}_b^T(s) \cdot \vec{\tilde{D}}_b(s)\, |h(s)|^3\, ds$$

$$\text{with} \qquad h_X(s) = h_0 + kX(s) \qquad h_Y(s) = -kY(s) \qquad |h(s)| = \sqrt{(h_X(s))^2 + (h_Y(s))^2}$$

$$C_x(s) = h_X(s)\left(|h(s)|^2 + 2k(s)\right) \qquad C_y(s) = h_Y(s)\left(|h(s)|^2 - 2k(s)\right) \qquad \bar{C}_x = |h_i|^2$$

The expressions are the same like on-axis, cf. 43.

The radiation integrals also include I_1, which actually is not related to radiation but describes the energy dependent path length. Including an energy offset u the path length element from eq. 59 becomes

$$dl = ds(1 + (h_X D_x + h_Y D_y)u)$$

Any higher orders of path length (i.e. non-linear momentum compaction) are contained in the local dispersion D_x.

Collecting our results we obtain Table I giving a summary of the contributions to the radiation integrals from a general (combined function) bending magnet with (constant) curvature h_0, quadrupole strength k and edge angles $\theta_{1,2}$ including coupling and orbit distortions. Our results agree with prior work by Sagan as documented in [15].

In the calculations we made the following assumptions and simplifications:

(a) The integrals extend along the displaced orbit. In a magnet of cylindrical symmetry with design curvature h_0, the integration path element thus becomes

$$dl = ds\,(1 + h_0 X(s)).$$

If the magnet further has a rotated edge of angle θ, then the path is shortened by

$$\Delta L = -X \tan\theta,$$

see Fig. 1. An integral over a function $f(s)$ thus becomes

$$\int_{\text{path}} f(s)\, dl = \int_{\Delta L_1}^{L-\Delta L_2} f(s)\,(1+h_0 X)\, ds \approx \int_0^L f(s)\,(1+h_0 X)\, ds - \sum_{i=1,2} f(s_i) \tan\theta_i\, X_i.$$

Basically this path length correction has to be applied to all radiation integrals. However, for storage rings operating at several GeV beam energy, the radius of curvature $\rho = 1/h_0$ is on the orders of meters, while the orbit excursion X is typically on the order of some millimeter. As a consequence, the path length modifications are a per-mill effect and may be neglected. For rectangular bends, as commonly used, where $\theta_1 = \theta_2 = h_0 L/2 \ll 1$ the two effects, lengthening of the path in the arc and shortening due to cut off by rotated edges, cancel anyway.

(b) It would be straightforward to extend the treatment to non-linear multipoles too, however the contribution to the integrals is rather small: the field increases quadratically (sextupole) or at even higher power with the distance from the axis, and the radiation integrals scale with the second or third power of the field. Even if the sextupoles are rather strong, like in a low-emittance storage ring, their contribution to the integrals is on a per-mill level compared to the quadrupole contribution – which in itself is a fraction of the bending magnet contribution – and thus may well be neglected.

(c) We only consider the design edge rotation (around the y-axis) of a bending magnet and neglect additional edge effects due to orbit slopes X', Y', because these angles are usually small compared to bending and edge angles. Thus the edge related path shortening does not depend on the vertical coordinates. Note that we only considered horizontal bending magnets, which may be sandwiched between rotations to model vertical or slanted deflections.

(d) During propagation the effect known as "mode flip" may occur: the normal mode decomposition locally may result in one or two solutions for the matrix T of Eq. 5. In strongly coupled lattices it can happen, that the solution in use does not exist anymore at the next element, and the other solution has to be used to propagate further, as described in [10]. In this case we proceed by adding the a-integrals to the b-sum integral of the ring and vice versa, until the originally used solution exists again. However, since we restricted

ourselves to regular magnets all changes of coupling (as expressed by the parameter g) occur at rotations, which are inserted before and after the magnets if needed, and no mode flip can occur during integration inside the magnet.

VII. APPLICATIONS

Several simulation codes are in use, e.g. MAD-X [16], elegant [17], AT [18], BMAD [19], Tracy [20], which incorporate different coupling formalisms [4]–[10] and calculate the equilibrium parameters for a given storage ring lattice. The code OPA [7] emerged from the former code OPTIK, which was written by K. Wille and colleagues at Dortmund university in the 1980's. The philosophy of the code was different providing an interactive, visual tool to build up a lattice from scratch like playing with LEGO$^{\mathrm{TM}}$ blocks, while restricting the models to elementary magnet types and functionalities.

For interactive lattice design from scratch it is convenient, although physically meaningless, to calculate radiation integrals even if it is not yet known if and how the lattice will be terminated or closed, i.e. irrespective of the existence of a periodic solution. For this purpose a forward propagation using analytical expressions for the integrals is required, which starts from initial beam parameters defining orbit, normal mode betas, coupling and dispersion. If a periodic solution exists, it will deliver the initial parameters and the same calculation can be applied. The OPA-code is based on this concept. Extending it to coupled lattices partially motivated the work described here.

The presented method to calculate the radiation integrals for the normal modes permits a straightforward implementation of the formulae in Table I: We assume that curvature h and gradient k are piecewise constant, then the transfer matrix R and the vector $\vec{V}$ of dispersion production in eq. 1 contain trigonometric or hyperbolic functions (to be found in any text book on accelerators, e.g.[3], [12], [13]), whereas otherwise analytic solutions can only be found for a few special cases of longitudinal field variation.

Constant h, k parameters can be extracted from the radiation integrals, and we are left with sums of definite integrals over multiple products of trigonometric or hyperbolic functions, which have elementary solutions. These solutions become rather lengthy and are not instructive at all, therefore we do not show them here. But they can be evaluated and exported as program code by a symbolic code, which was the first and most efficient

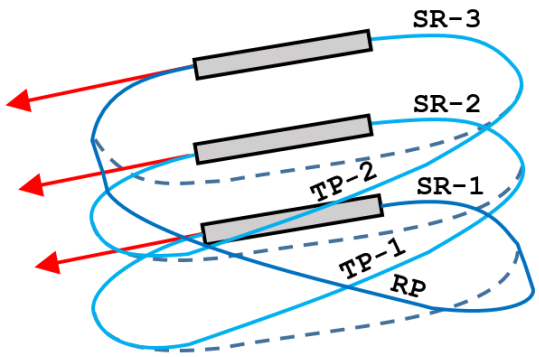


FIG. 2. Schematic layout of the Spiral-COSAMI lattice (from [8]).

implementation. Solving the integrals numerically by dividing the magnets into sufficiently small slices instead of evaluating the analytical solutions is less elegant and computationally more expensive, but easy and straightforward to implement and to extend further, in order to also include orbit distortions, longitudinal field variations etc.

Linear beam optics is calculated from the local transfer-matrix, which is the Jacobian of the non-linear map at the orbit position. The orbit itself is the fixpoint of the one-turn map in a periodic system, or just the propagation of initial conditions including all multipoles in a single-pass system. Off-axis down-feeds have to be included in linear optics, like the additional dispersion production on the displaced orbit, $\Delta\vec{D}(s) = d\vec{X}(s)/du|_{u=0}$, and local quadrupole and skew quadrupole gradients from non-linear multipoles.

Implementation details and practical issues will be described elsewhere [7]. In the following we will show four example applications:

Example 1: The Spiral-COSAMI storage ring is a machine for industrial application of extreme ultraviolet light [8]. It is build from three vertically stacked turns as sketched in Fig. 2. The tilting of the arcs introduces coupling and excites a wave of vertical dispersion as shown in Fig. 3. The figure shows the normal mode beta functions which almost coincide with the projections to physical x, y space since coupling is low. The physical dispersions also shown in the figure are defined in the local coordinate system and thus show discontinuities at locations of coordinate rotation. The normal mode equilibrium emittances of this lattice amount to 3.43/0.23 nm at 430 MeV. This result was confirmed by the code TRACY [20], which employs a different method of emittance calculation based on the 6-dimensional periodic sigma-matrix [21].

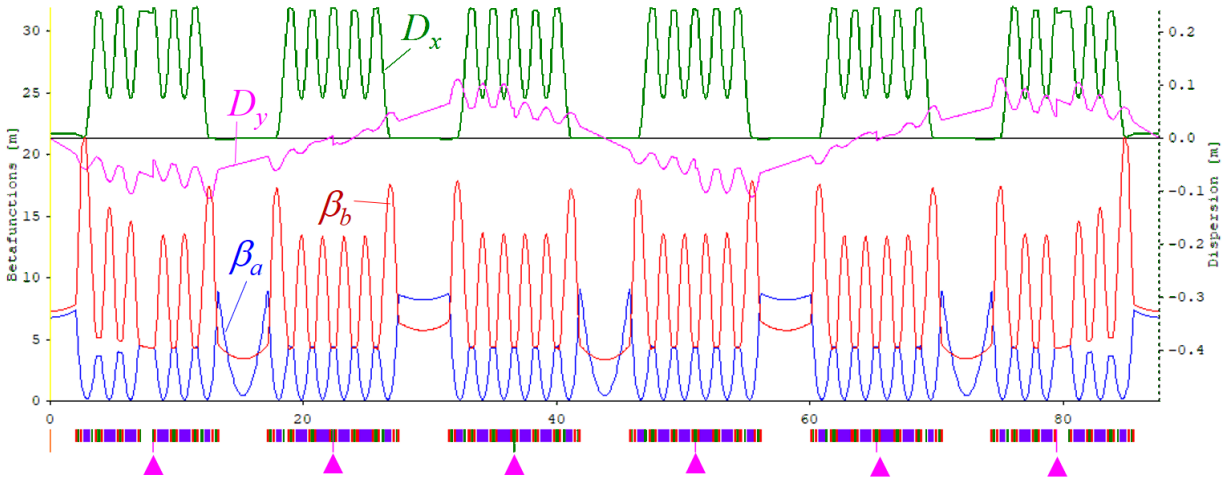


FIG. 3. Optics of the Spiral COSAMI lattice showing normal mode beta functions (left axis) and physical dispersions (right axis). The triangles at the bottom indicate points of rotations by angles $\{-\beta, \alpha, \alpha, \alpha, \alpha, -\beta\}$ with $\alpha = 3.86°$, $\beta = 7.69°$

Example 2: The lattice for the upgrade of the Swiss Light Source, SLS 2.0 [22] has a natural horizontal emittance of 158 pm at 2.7 GeV. 264 skew quadrupoles are set to generate closed bumps of vertical dispersion in the arcs in order to create 10 pm of b-mode emittance, which is a compromise between beam life time due to Touschek scattering and photon beam brightness. Due to the rather low coupling the vertical emittance basically is given by the b-mode emittance. Closing all undulators to minimum gaps increases the radiated power as given by the I_2-integral while little affecting the other integrals, and thus reduces the normal mode emittances to 134 pm and 7.7 pm. Scaling all skew quadrupoles by the same factor proportional to $\sqrt{I_2}$ keeps the b-mode emittance at 10 pm for the fully loaded lattice. Fig. 4 shows the normal mode beta functions β_a, β_b and the physical dispersions D_x, D_y for one super-period of the fully loaded, ideal lattice. Fig. 5 demonstrates for the unloaded lattice how the vertical emittance increases due to orbit distortion when exciting one vertical corrector. We tracked the residual discrepancy between the results from TRACY and OPA to slightly different methods to calculate the off-axis dispersion.

Example 3: As an example of an extremely coupled machine we designed a ring in which we can continuously adjust the coupling between an uncoupled configuration and a Möbius

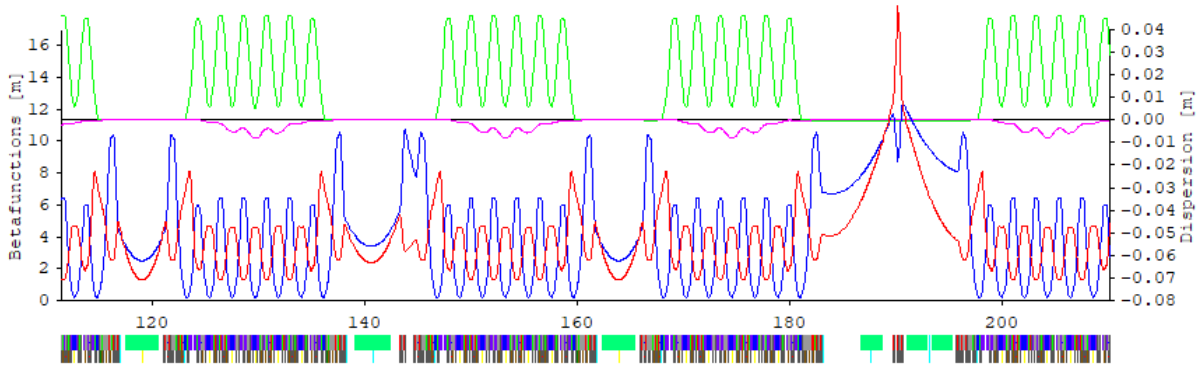


FIG. 4. Normal normal mode beta functions (blue a-mode, red b-mode) and dispersions (green horizontal, magenta vertical) for setors 6 to 9 of the SLS 2.0 lattice loaded with insertion devices.

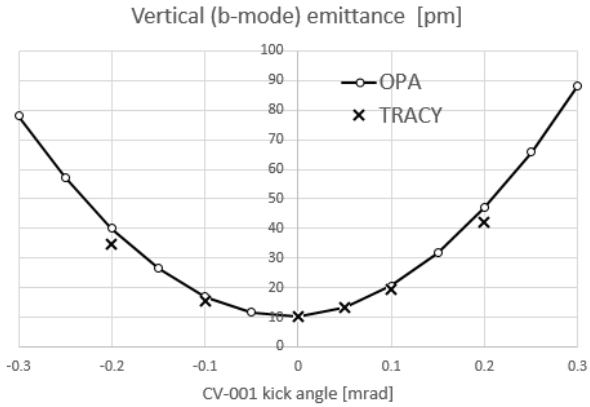


FIG. 5. Comparison of OPA- and TRACY calculations of vertical emittance due to orbit distortion, if one vertical corrector is excited (located at $\beta_y = 7.6\ m$).

configuration [23], where the transverse planes are exchanged after one turn. This racetrack-shaped ring [24] is based on 10 m long FODO cells with 90° phase advance in both planes. In the two arcs the phase advance in the vertical plane is slightly reduced in order to split the integer tunes, while the phase advance in the horizontal plane remains at 90°, which allows us to implement a dispersion suppressor with four half-length dipoles. The two straight sections consist of six 90° FODO cells. One is used to adjust tunes and the other implements a Möbius tuner with three skew quadrupoles placed in the middle of corresponding drifts spaces in consecutive cells [25]. This ensures that the phase advance between consecutive skew quadrupoles is 90° in both planes. If we now choose the focal length of the skew quadrupole to be equal to the beta function in the middle of the straight, the transfer matrix for this section has 2×2 blocks with zeros on the diagonal and non-zero entries in

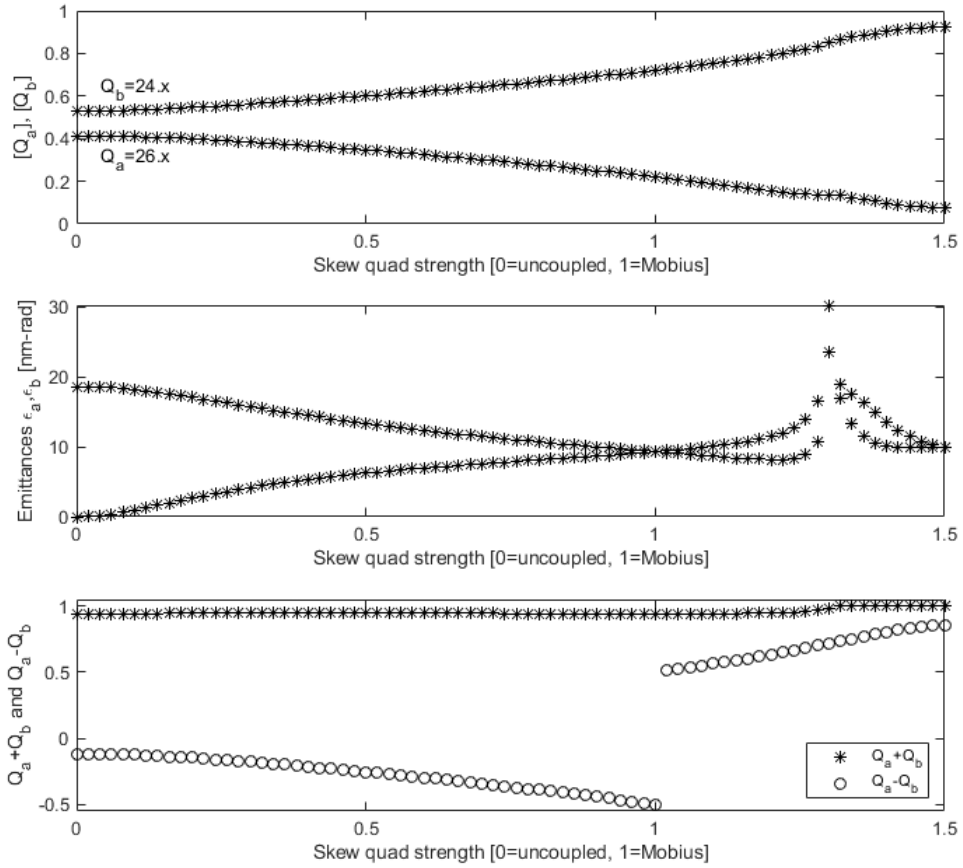


FIG. 6. The fractional tunes (top) and the emittances (middle) of the Möbius ring (top) as a function of the excitation of the skew quadrupoles. The bottom panel shows the sum and difference of the tunes.

the off-diagonal blocks. In other words, it exchanges the transverse planes. Adjusting the excitations of the three skew quadrupoles by the same factor allows us to continuously vary the coupling between an uncoupled ring and one in the Möbius configuration.

The upper panel in Figure 6 shows the fractional tunes for the ring as the excitation of the skew quadrupoles is increased from zero to the Möbius configuration and up to 1.5 times that excitation. The integer part of the tune is indicated on the left-hand side of the plot. We see that increasing the excitation of the skew quadrupoles "pushes the fractional tunes apart", which makes it beneficial to place one tune above the half-integer and the other below. This prevents the crossing of the half integer with the ensuing instability for one of

the tunes. The middle panel shows the emittances calculated with Eq. 52. We observe that increasing the excitation of the skew quadrupoles to the Möbius configuration reduces one of the emittances and increases the other one such that they become equal. The lower panel shows that the difference between the fractional part of the tunes becomes half-integer at this point. Increasing their excitation further causes both emittances to increase dramatically. The plot on the lower panel provides an explanation; the sum of the tunes $Q_a + Q_b$ becomes an integer and the system crosses a sum resonance shown by the asterisks in the lower panel from Figure 6. And on a sum resonance, the emittances can become arbitrarily large, because only their difference is bounded (Sec.2.1.3 in [12]).

Example 4: A Möbius insertion in a light source is an option to lower the bunch density in order to minimize emittance growth and particle losses (Touschek effect) due to intra-beam scattering. Furthermore, some beam lines prefer photon beams of almost round cross section obtained in this way. Our last example demonstrates application to the SLS 2.0 lattice: The Möbius insertion could be realized in one of the of the short straight sections. It is made from five skew and two regular quadrupoles [25]. Figure 7 shows the optical functions in magnification: normal mode beta functions jump at the location of the (thin) skew quadrupoles, whereas their projections to x- and y-axes, which correspond to the physical beam envelopes, vary continuously. Outside the Möbius insertion the projections from the a- and b-modes to x, resp. to y coincide, indicating full coupling at $g = \sqrt{1/2}$. As a consequence the radiation integrals for both modes are identical, and so are the damping times and the emittances. The uncoupled lattice without insertion devices has a natural emittance of $\epsilon_{xo} = 158$ pm and damping partitions of $\mathcal{J}_{xo} = 1.828$, $\mathcal{J}_{yo} = 1.000$. The Möbius lattice has $\mathcal{J}_a = \mathcal{J}_b = (\mathcal{J}_{xo} + \mathcal{J}_{yo})/2 = 1.414$ and emittances of $\epsilon_a = \epsilon_b = \epsilon_{xo}/(1 + \mathcal{J}_{yo}/\mathcal{J}_{xo}) = 102$ pm. These result in projected emittances of same amount, $\epsilon_x = \epsilon_y = 102$ pm outside the insertion, whereas projected emittances are larger inside the insertion.

VIII. CONCLUSION

We found a generalization of the synchrotron radiation integrals that are responsible for the emittance growth in coupled lattices. It turned out that the resulting methodology is rather intuitive. It consist of projecting the four dimensional coupled dispersion from eq. 8

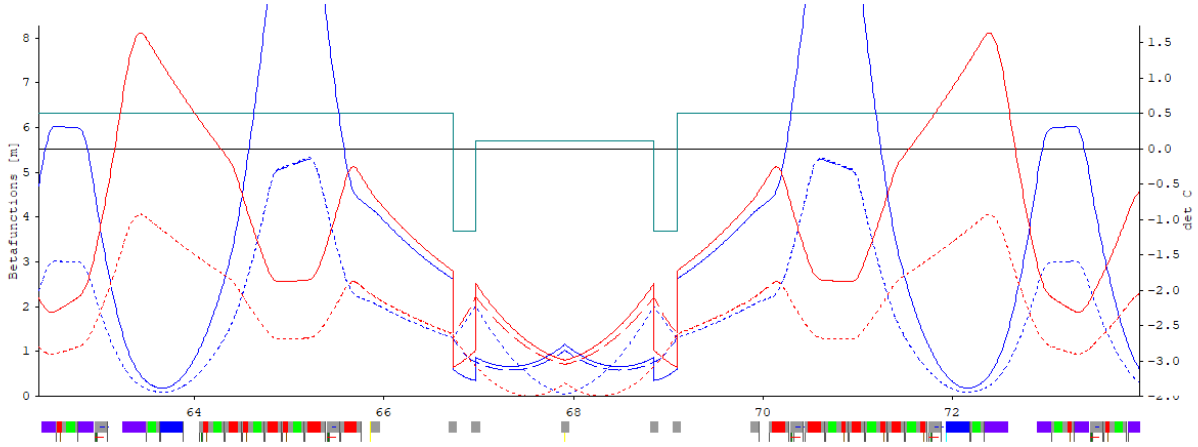


FIG. 7. Möbius insertion in straight 4 of the SLS 2.0 storage ring. Solid lines show the normal mode betafunctions (blue a-mode, red b-mode), dashed and dotted lines the projected beta functions β_{xa}, β_{yb} and β_{xb}, β_{ya} (blue β_x, red β_y). The square line shows the determinant of the coupling matrix $\det C = 1 - g^2$ (axis at right).

onto the normal modes that are constructed from the Edwards-Teng formalism. Then the emittance growth integral is given through the normal-mode beta functions and dispersion $\vec{\vec{D}}$. The same method also worked to project the effect of damping due to the emission of synchrotron radiation on to the normal modes. The formalism allows off-axis contribution to be included, and implementation in a beam dynamics code is straightforward. In this way the formalism allows to introduce the coupling of the normal-mode emittances in a natural way.

ACKNOWLEDGEMENTS

We would like to thank Masamitsu Aiba (PSI) for setting up the Möbius insertion in the latest SLS 2.0 lattice, and for useful discussions, and Michael Böge (PSI) and Bernard Riemann (PSI) to perform cross-checks of our example applications using the TRACY code. We further gratefully acknowledge helpful comments from David C. Sagan (Cornell University).

[1] M. Sands, Conf. Proc. **C6906161**, 257 (1969).

[2] R. H. Helm, M. J. Lee, P. L. Morton, and M. Sands, IEEE Trans. Nucl. Sci. **20**, 900 (1973).

[3] D. Edwards and M. Sypers, *An Introduction to the Physics of High Energy Accelerators* (John Wiley & Sons, Inc., New York, 1993).

[4] A. W. Chao, J. Appl. Phys. **50**, 595 (1979).

[5] K. Ohmi, K. Hirata, and K. Oide, Phys. Rev. **E49**, 751 (1994).

[6] A. Wolski, Phys. Rev. ST Accel. Beams **9**, 024001 (2006).

[7] OPA, *Project web site:* `http://ados.web.psi.ch/opa/`.

[8] A. Wrulich, A. Streun, and L. Rivkin, Nucl. Instrum. Meth. A **1014**, 165731 (2021).

[9] D. Edwards and L. Teng, IEEE Transactions on Nuclear Science **20**, 885 (1973).

[10] D. Sagan and D. Rubin, Phys. Rev. ST Accel. Beams **2**, 074001 (1999), [Phys. Rev. ST Accel. Beams3,059901(2000)].

[11] V. Ziemann, *Hands-On Accelerator Physics Using MATLAB®* (CRC Press, 2019), 1st ed.

[12] F. Zimmermann, K. Mess, and M. Tigner, *Handbook of Accelerator Physics and Engineering* (World Scientific, 2013), 2nd ed.

[13] S. Y. Lee, *Accelerator Physics* (World Scientific, 2004), 2nd ed.

[14] K. W. Robinson, Phys. Rev. **111**, 373 (1958), [205(1958)].

[15] D. Sagan, *The BMAD reference manual [19].*

[16] MADX, *Project web site:* `http://madx.web.cern.ch/madx/`.

[17] ELEGANT, *Project web site:* `https://ops.aps.anl.gov/elegant.html`.

[18] AT, *Project web site:* `http://atcollab.sourceforge.net/`.

[19] BMAD, *Project web site:* `https://www.classe.cornell.edu/bmad/`.

[20] TRACY, *Project web site:* `https://github.com/jbengtsson/tracy-3.5/`.

[21] A. W. Chao, Journal of Applied Physics **50**, 595 (1979).

[22] H. Braun, T. Garvey, M. Jörg, A. Ashton, P. Wilmott, and R. Kobler, *SLS 2.0 storage ring technical design report, PSI 2021,* `https://www.dora.lib4ri.ch/psi/islandora/object/psi:39635`.

[23] R. Talman, Phys. Rev. Lett. **74**, 1590 (1995).

[24] V. Ziemann, *Beam parameters in a Möbius ring, FREIA Report 2022/01, Jan. 2022,* `https://arxiv.org/abs/2201.01083`.

[25] M. Aiba, M. Ehrlichman, and A. Streun, in *Proc. IPAC 2015, Richmond VA, USA* (2015), pp. 1716–1719.